ACS APPLIED MATERIALS & INTERFACES

Research Article

www.acsami.org

Graphene-Induced Oriented Interfacial Microstructures in Single Fiber Polymer Composites

John P. Abdou, Gregory A. Braggin, Yanqi Luo, Alexandra R. Stevenson, Danielle Chun, and Shanju Zhang*

Department of Chemistry and Biochemistry, California Polytechnic State University, 1 Grand Avenue, San Luis Obispo, California 93407, United States

Supporting Information

ABSTRACT: Interfacial interactions between the polymer and graphene are pivotal in determining the reinforcement efficiency in the graphene-enhanced polymer nanocomposites. Here, we report on the dynamic process of graphene-induced oriented interfacial crystals of isotactic polypropylene (iPP) in the single fiber polymer composites by means of polarized optical microscopy (POM) and scanning electron microscopy (SEM). The graphene fibers are obtained by chemical reduction of graphene oxide fibers, and the latter is produced from the liquid crystalline dispersion of graphene oxide via a wet coagulation route. The lamellar crystals of iPP grow perpendicular to the fiber axis, forming an oriented transcrystalline (TC) interphase surrounding the graphene fiber. Various factors including the diameter of graphene fibers, crystallization temperature, and time are investigated. The dynamic process of polymer transcrystallization surrounding the graphene fiber is studied in the temperature range 124−132 °C. The Lauritzen−Hoffman theory of heterogeneous nucleation is applied to analyze the transcrystallization process, and the fold surface free energy is determined. Study into microstructures demonstrates a cross-hatched lamellar morphology of the TC interphase and the strong interfacial adhesion between the iPP and graphene. Under appropriate conditions, the β-form transcrystals occur whereas the α-form transcrystals are predominant surrounding the graphene fibers.

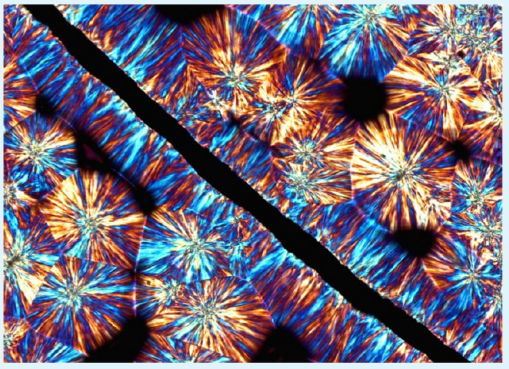

KEYWORDS: *graphene, polymer composites, interfacial interactions, crystallization kinetics, fibers, adhesion*

INTRODUCTION

Graphene is a single-atom-layer of sp^2-hybridized carbon in a two-dimensional (2D) lattice, exhibiting exceptional mechanical, electronic, and thermal properties.[1−3] One of the most promising applications is to serve as a reinforcing agent in the polymer matrices for the production of functional nanocomposites.[4−10] Because of the molecular sized dimension and large specific surface areas, a small amount of graphene can substantially enhance mechanical performance, gas barrier, rheological properties, thermal behaviors, and electrical conductivities of the polymer matrices.[11−13] Interestingly, the graphene-reinforced polymer composites often exhibit unprecedented intriguing properties due to the synergistic effects of their components,[7] which are expected to overcome the fundamental limitations of current energy storage and conversion.

It has been recognized that the interfacial interactions between the host polymer and nanofillers are pivotal in improving the interfacial adhesion and thereafter the physical properties of resulting nanocomposites.[14−17] Recently, large efforts have been made to improve interfacial bonding between the polymer and graphene using both chemical and physical methods.[18−20] In particular, graphene in semicrystalline polymer matrices can serve as a heterogeneous nucleating agent for accelerating polymer crystallization.[10,21−24] The resulting interfacial crystalline structures and morphologies are significantly different from those in the bulk in terms of the crystal size, chain conformation, chain packing, and chain mobility.[24] Such interfacial crystallization offers an effective way to enhance the interfacial adhesion and stress transfer.[25−27] However, it remains challenging to directly visualize the interfacial morphology on the nanofillers without high resolution experimental methods.

The fiber-reinforced polymer composites have been well-investigated. The most commonly used method for studying the interfacial morphology between the polymer and fibers via optical microscopy is to fabricate single fiber polymer composites.[28−33] Typically, a single fiber is embedded in the polymer matrix, followed by isothermal melt crystallization. The fiber surfaces force the polymer crystal growth perpendicular to the fiber axis. The resulting oriented interfacial crystals form a columnar layer around the fiber, which is termed as a transcrystalline (TC) layer.[28] It is evident that polymer transcrystallization not only improves the interfacial adhesion

Received: April 16, 2015
Accepted: May 29, 2015
Published: June 9, 2015

DOI: 10.1021/acsami.5b03269
ACS Appl. Mater. Interfaces 2015, 7, 13620−13626

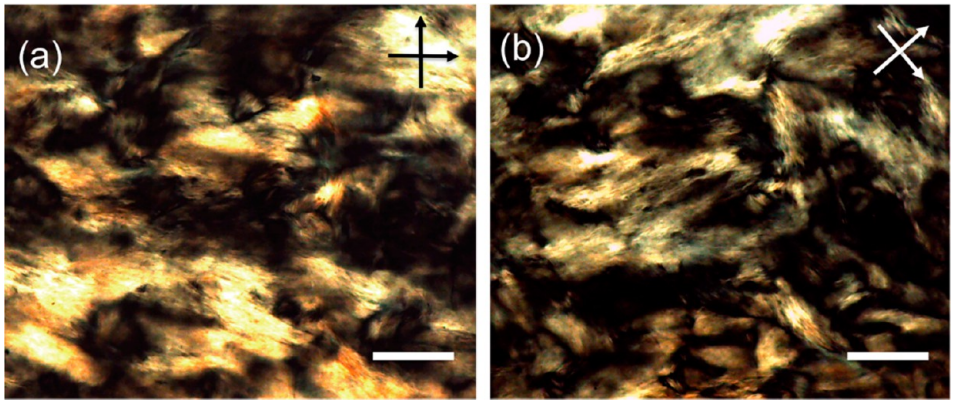

Figure 1. Liquid crystalline (LC) textures of aqueous dispersion of GO sheets at 10 mg/mL under polarized optical microscope: (a) 0° rotation and (b) 45° rotation. The LC polydomains become bright and dark as the crossed polarizers rotate. The scale bar represents 200 μm.

and stress transfer, but also changes polymer crystal structures.[28] Recent advances in graphene allow the fabrication of macroscopic graphene oxide (GO) fibers that can be transformed into reduced graphene oxide (rGO) fibers or graphene fibers via thermal or chemical reduction.[34−36] Graphene fibers provide new ways to study interfacial interactions between the polymer and graphene for producing high performance graphene-enhanced polymer nanocomposites. However, to the best of our knowledge, there have been no reports on polymer transcrystallinity induced by the graphene fibers. In this work, we report on the dynamic process of transcrystallization of iPP surrounding the graphene fibers by means of polarized optical microscopy (POM) and scanning electron microscopy (SEM).

EXPERIMENTAL SECTION

Synthesis of Graphene Oxide. Graphene oxide (GO) was synthesized from natural graphite flakes via a modified Hummers method.[37,38] Typically, 1.0 g of graphite flakes was mixed with 40 mL of the acid mixture of 98% H_2SO_4 and 70% HNO_3 at a volume ratio of 3:1 under stirring at room temperature for 24 h. The acid-treated graphite flakes were then rinsed with deionized (DI) water to get pH = 5. The dried sample was heat-treated in a furnace at 1050 °C for 10 s to get expanded graphite (EG) flakes. The EG flakes and 200 mL of 98% H_2SO_4 were mixed and stirred at 0 °C, and then 10 g of $KMnO_4$ was added. The mixture was then heated to 40 °C and stirred violently for 4 h. The system was then transferred to an ice bath, and 200 mL of DI water was added to the mixture, followed by dropwise addition of 3 mL of 30% H_2O_2. The resulting dispersion was centrifuged with 1.0 M HCl solution to produce a bright yellow paste. The paste was further washed with DI water until the pH became about 5. After centrifugation, a gel-like dispersion of GO was received.

Wet Spinning of Graphene Oxide Fibers. A 10 mg/mL aqueous dispersion of GO was loaded into a syringe and extruded by a syringe pump at ~3 mL min^{-1} into the bath of 5% $Zn(NO_3)_2$ in ethanol. The fibers were then collected on the Teflon rod outside the bath and dried under infrared (IR) light. The dried GO fibers were immersed into an aqueous solution of 30% hydroiodic acid (HI) at room temperature overnight. The reduced graphene oxide (rGO) fibers were then rinsed by DI water and ethanol, and dried under infrared light.

Preparation of Single Fiber Composites. The rGO fibers were introduced into the film of isotactic polypropylene (iPP) and hot pressed at 200 °C for 5 min to erase thermal history of the sample. The sample was then cooled at a rate of 20 °C min^{-1} to the isothermal crystallization temperature that was in the range from 124 to 132 °C.

Characterization. Fourier transform infrared (FTIR) spectra of GO and rGO were obtained on a Nicolet iS10 FT-IR spectrometer in an attenuated total reflection (ATR) mode at a resolution of 8 cm^{-1} of 1000 scans. Thermogravimetric analysis (TGA) data were collected on a TA Instruments Q500 in air at a heating rate of 10 °C min^{-1}. The X-ray analysis was taken on reflection geometry Siemens D5000 diffractometer with a 1.54 Å Cu Kα radiation source. The liquid crystal textures were evaluated on a Leica DM2500P polarized optical microscope (POM). The Leica ICC50 HD video camera was applied to record the dynamic transcrystallization process under the microscope connected with a Linkam LTS420 hot-stage. The hot-stage was programmed using the Linksys32 software to control the temperature. Scanning electron microscopic (SEM) images were received on a FEI Quanta 200 microscope operated at an acceleration voltage of 20 kV. To reveal the transcrystalline morphology under SEM, the samples were etched for 2 h with a 1.0 wt % solution of $KMnO_4$ in a 2:1 acid mixture of 98% H_2SO_4 and 85% H_3PO_4 under ultrasonication. The etched samples were then coated with a fine gold layer by sputtering.

RESULTS AND DISCUSSION

We synthesized the exfoliated GO sheets from natural graphite flakes using a modified Hummers method.[37,38] The resulting GO sheets possessed a variety of oxygen-based functional groups, including carboxylic acid, hydroxyl, and epoxy groups. The chemical structure of GO sheets was evidenced by the data of FTIR and TGA (Supporting Information Figure S1). As-prepared GO sheets were then dispersed in DI water with various concentrations. Interestingly, the phase transition from isotropic to liquid crystalline (LC) phases was observed under POM when the concentration was above 3.5 mg/mL. Figure 1 shows representative optical images of aqueous dispersions of GO sheets at 10 mg/mL. The strong optical birefringence with black brush patterns demonstrates typical Schlieren textures of a polydomain LC phase.[39] Upon 45° rotation of the crossed polarizers, the bright and dark regions change alternately resulting from the relative alignment of the LC director and the polarization vector of the light (Figure 1a,b). The observed LC behavior of aqueous dispersions of GO sheets is consistent with recent literature reports.[34,37,40,41]

Figure 2a illustrates the schematic of LC spinning of GO fibers via a wet coagulation route. Typically, the LC dope was extruded by a syringe pump through a long capillary spinneret into a coagulation bath of 5% $Zn(NO_3)_2$ in ethanol. During the extrusion, the GO sheets in the LC phase were forced to align by the pressure-driven flow. As a result, the polydomain LC dope was transferred into the single domain gel fiber (Supporting Information Figure S2). In the coagulation bath, the water rapidly diffused out of the extruded fiber into the bath with ethanol back-diffusing into the fibers. The ethanol-swollen

DOI: 10.1021/acsami.5b03269
ACS Appl. Mater. Interfaces 2015, 7, 13620−13626

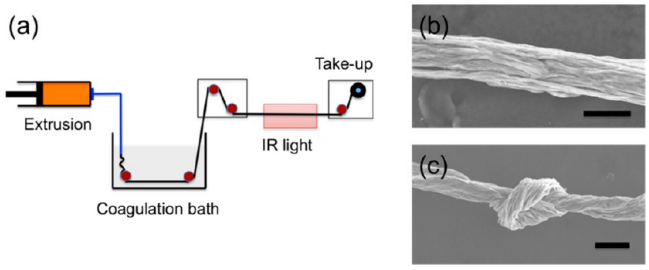

Figure 2. Wet coagulation of GO fibers spun from the LC dispersion: (a) schematic diagram of a homemade fiber setup, (b) SEM image of the GO fiber, and (c) SEM image of tying knot of the GO fiber. The scale bar represents 20 μm.

GO fiber was then removed out of the coagulation bath and dried under infrared (IR) light. As-spun GO fibers are 30−80 μm in diameter depending on the spinning conditions, and GO sheets are wrinkled as revealed under SEM (Figure 2b). The fibers are flexible and readily knotted by hand (Figure 2c). This knotting property is important for the weaving and knitting of technical textile fibers. The GO fibers were then reduced by 30% HI. The resulting reduced GO fibers (here it is referred as graphene fibers) inherited the morphology of the GO fibers (Supporting Information Figure S3), and their structures were confirmed by FTIR and TGA measurements (Supporting Information Figure S1).

Figure 3 displays typical optical images of a single graphene fiber/iPP composite in the quiescent melt at 132 °C. The oriented crystalline lamellae surrounding the graphene fiber are apparent, which is identified as a transcrystalline (TC) interphase.[28] Upon rotation of the sample in the presence of a retardation plate under the crossed polarizers, the blue and orange contrast of the mixed birefringence TC interphase changes accordingly. Away from the graphene fiber, the spherulitic structures of iPP in the bulk are predominant. This TC morphology bears the resemblance to those obtained in the single carbon fiber composites[28] and single CNT fiber composites.[42,43] As a comparison, the single GO fiber/iPP composites were prepared and isothermally crystallized under the same conditions. As expected, the GO fibers failed to promote the TC microstructures of iPP (Supporting Information Figure S4). In this case, the weak capacity of the GO fibers for nucleating iPP may be attributed to the mismatch of the surface energy between the hydrophilic GO sheets (62 mJ/m^2)[44] and the hydrophobic iPP matrix (30 mJ/m^2).[45]

Figure 4 shows the TC textures of iPP with different size graphene fibers that were treated under the same conditions. With increasing size of graphene fibers, the fiber surface becomes rough, which is evidenced by SEM images (Supporting Information Figure S3). On the other hand, the larger fibers possess smaller surface-to-volume ratios. Interestingly, polymer transcrystallization occurs in all cases regardless of the fiber size. Further investigation is warranted in this context.

To understand the formation mechanism of the TC interphase in the single graphene fiber/iPP composites, the dynamic process of polymer transcrystallization has been investigated at 132 °C using in situ POM (Figure 5). It is evident that the graphene fiber promotes fast iPP nucleation, forming a bright layer of TC nuclei (Figure 5b). This observation is indicative of the high nucleating capacity of the graphene fiber toward the iPP matrix.[42] Over time, the aligned crystalline lamellae grew perpendicular to the fiber axis, forming a TC interphase surrounding the graphene fiber (Figure 5c−f). Finally, the growth of the TC interphase was interrupted by the iPP spherulites grown in the bulk (Figure 5f). To this end, video microscopy was employed to record the TC interphase during the isothermal crystallization at different crystallization temperatures. The thickness of the TC interphase was then analyzed using ImageJ to study the transcrystallization kinetics.

Figure 6a shows the growth of the TC interphase over time in the temperature range 124−132 °C. The linear relationship between the thickness of the TC interphase and time was found over the entire temperature range investigated. In this regard, the growth rate (G) of the TC interphase at each temperature was obtained from the slope of the plot. As expected, decreasing temperature promotes the nucleation with smaller induction time and thus accelerates the transcrystallization process with a high growth rate.[46]

According to the Lauritzen−Hoffman theory of heterogeneous nucleation,[47] the growth rate (G) is determined by eq 1

$$G = G_0 \exp\left(\frac{-U^*}{R(T_c - T_\infty)}\right)\exp\left(\frac{-K_g}{T_c \Delta T}\right) \quad (1)$$

where G_0 is the pre-exponential constant that contains all temperature-independent parameters, U^* represents the activation energy for the polymer transport across the phase boundary, R is the universal gas constant, T_c denotes the isothermal crystallization temperature, $T_\infty = T_g - 30$ (T_g is the glass transition temperature), $\Delta T = T_m^0 - T_c$ (T_m^0 is the melting

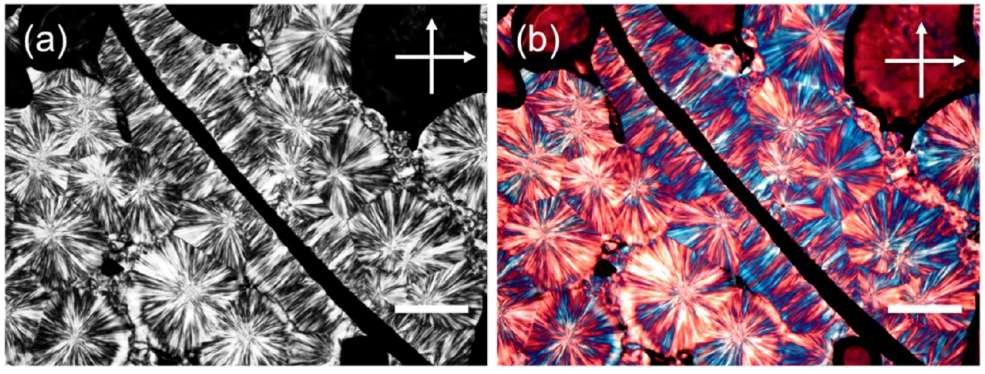

Figure 3. Optical micrographs of a single graphene fiber/iPP composite crystallized at 132 °C for 30 min. Transcrystals surrounding the graphene fiber under crossed polarizers: (a) without and (b) with the retardation plate. The scale bar represents 200 μm.

DOI: 10.1021/acsami.5b03269
ACS Appl. Mater. Interfaces 2015, 7, 13620−13626

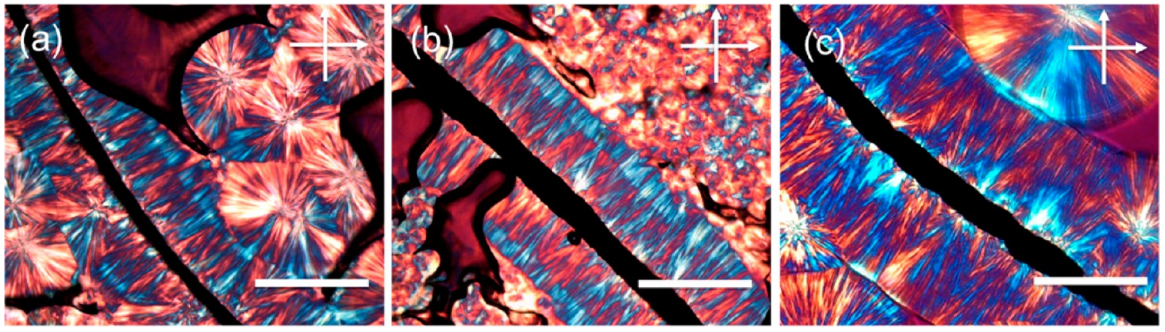

Figure 4. Polarized optical micrographs with retardation plates of iPP transcrystals crystallized at 132 °C surrounding the graphene fibers with different diameters: (a) 30, (b) 50, and (c) 70 μm. The scale bar represents 200 μm.

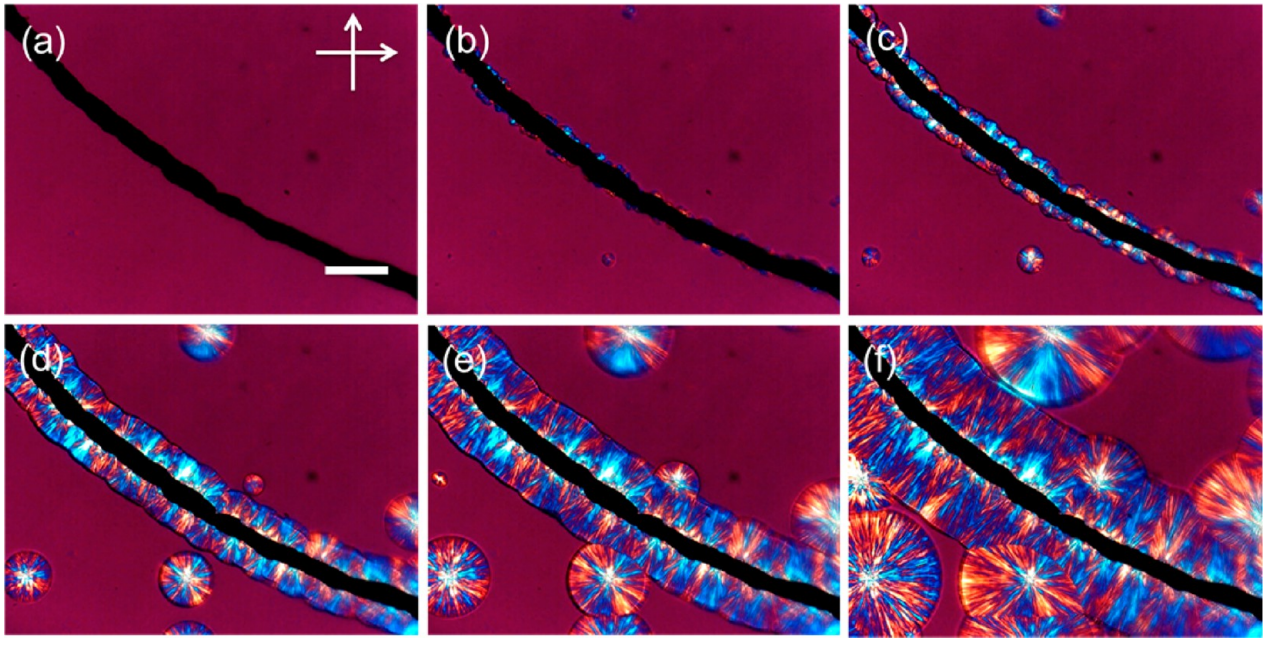

Figure 5. Series of polarized optical micrographs with retarding plates of iPP transcrystal evolution surrounding a single graphene fiber at 132 °C with different crystallization times: (a) 0, (b) 3, (c) 6, (d) 12, (e) 18, and (f) 30 min. The scale bar represents 200 μm.

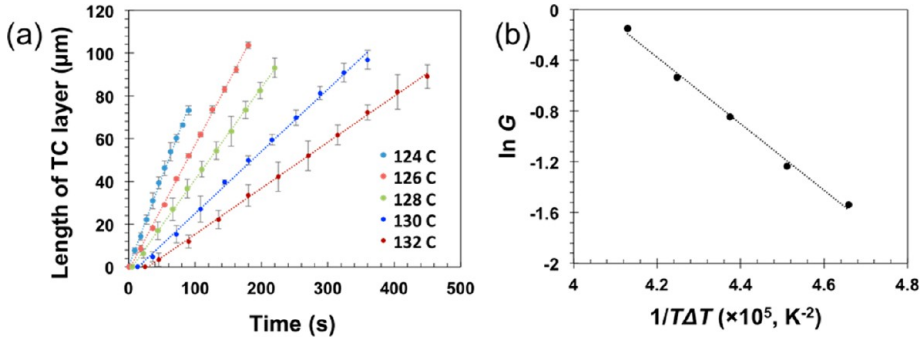

Figure 6. Kinetics of transcrystallization of iPP induced by the graphene fibers. (a) The plots of transcrystal (TC) thickness versus time at different crystallization temperatures T_c as shown in the figure, and (b) the plot of the growth rate (G) of transcrystals versus $1/(T_c\Delta T)$. $\Delta T = T_m^0 - T_c$, and is the supercooling degree, and T_m^0 is the melting temperature at equilibrium.

temperature at equilibrium), and K_g is the nucleation constant that is determined by the fold surface free energy. The first exponential term in eq 1 represents the diffusion process of the polymer chain segments in melt, while the second exponential term is associated with the thermodynamic driving force of chain-folding during the heterogeneous nucleation process.[47] For polymer transcrystallization, the second exponential term is predominant over the first one.[42,46] In this regard, the growth rate (G) of the TC interphase is mainly dependent on $1/(T_c\Delta T)$. Equation 1 is then simplified and expressed by eq 2

$$\ln G = -\frac{K_g}{T_c\Delta T} + \text{constant} \quad (2)$$

DOI: 10.1021/acsami.5b03269
ACS Appl. Mater. Interfaces 2015, 7, 13620−13626

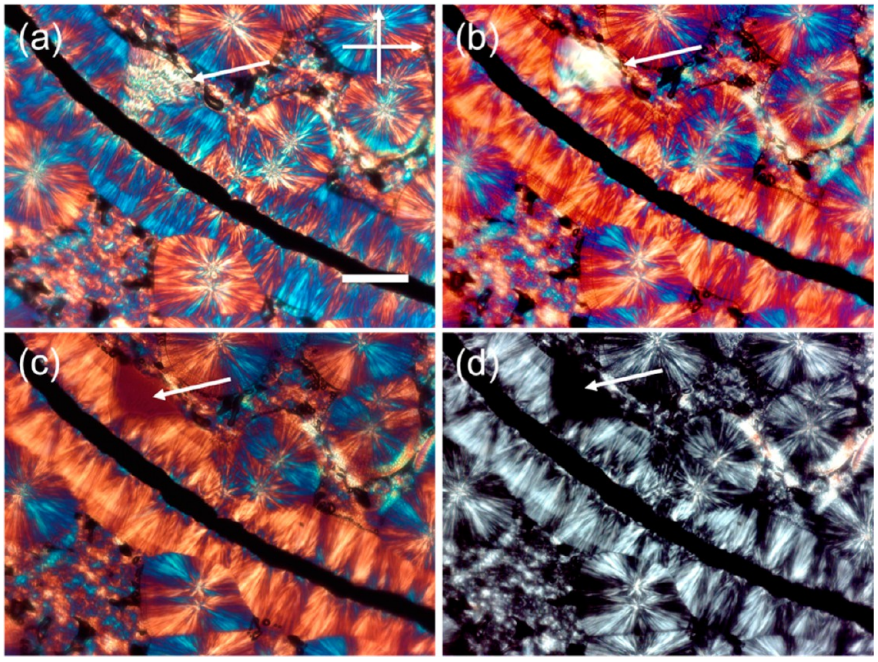

Figure 7. Polarized optical micrographs of the polymorphous transcrystals of iPP surrounding a single graphene fiber. The sample was isothermally crystallized at 132 °C for 30 min with subsequent quenching to room temperature: (a) as-prepared sample with a retarding plate, (b) the same sample from part a at the selective melting temperature of 155 °C with a retarding plate, (c) the same sample from part a at the selective melting temperature of 161 °C with a retarding plate, and (d) the same sample as that from part c without a retarding plate. The arrows show the β-form transcrystals. The scale bar represents 200 μm.

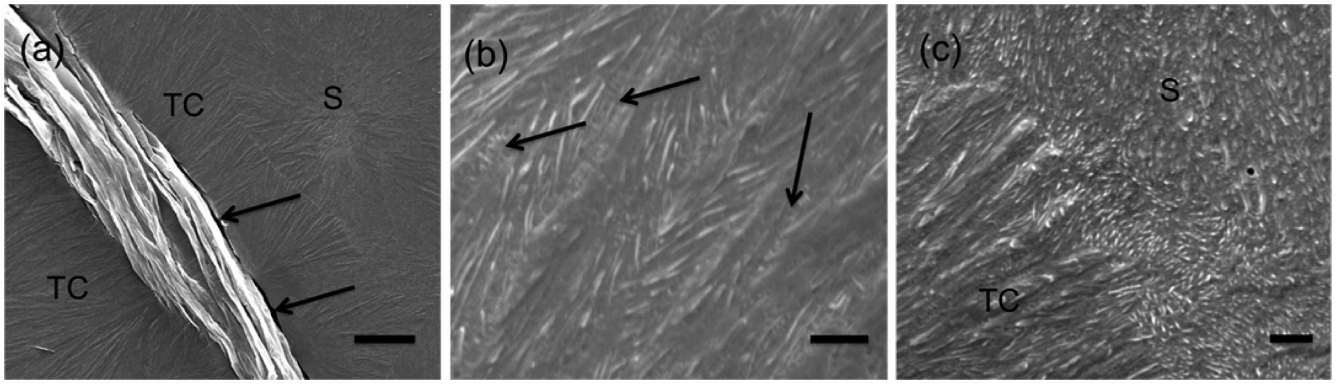

Figure 8. SEM images of transcrystallized polypropylene surrounding the graphene fiber after chemical etching: (a) overall morphology of single graphene fiber/polypropylene composite, (b) the transcrystalline interphase, and (c) the boundary between the transcrystalline interphase and bulk spherulites. TC and S represent transcrystals and spherulites, respectively. The scale bar represents 10 μm in part a and 800 nm in parts b and c.

Figure 6b shows the plot of ln G versus $1/(T_c\Delta T)$. The best-fit straight line was apparent. From the slope of the straight line, the K_g of 2.62 × 10^5 K^2 was then calculated. The K_g is the energy term for the formation of crystal nuclei with the critical size and is determined by eq 3

$$K_g = \frac{4b_0\sigma\sigma_e T_m^0}{k_B \Delta h_f} \quad (3)$$

where b_0 denotes the thickness of molecular monolayer in the polymer crystals, σ and σ_e represnt the lateral and fold surface free energies, respectively, k_B is the Boltzmann constant, and Δh_f is the heat of fusion per unit volume of the polymer crystals. It has been reported that, for α-form crystals of iPP,[48] b_0 is 6.26 Å, σ is 1.10 × 10^{-2} J m^{-2}, T_m^0 is 458 K, and Δh_f is 209 J g^{-1}. From these values and eq 3, the $\sigma\sigma_e$ was calculated to be 6.24 × 10^{-4} J^2 m^{-4}, and thus, the σ_e was 5.42 × 10^{-2} J m^{-2}. This value of the fold surface free energy is in good agreement with that (6.8−7.6 × 10^{-2} J m^{-2}) of the single CNT fiber/iPP composites[42,43] and that (4−11 × 10^{-2} J m^{-2}) of single carbon fiber/iPP composites.[49]

It is interesting to note that some fan-shaped domains were frequently observed in the TC interphase as indicated by an arrow in Figure 7a. Significantly, such fan-shaped domains display much stronger optical birefringence compared to the surrounding TC interphase and are thus identified by the β-form crystals of iPP.[50] The preliminary data of XRD analysis confirmed the existence of the small amount of the β-form crystals of iPP in the predominant α-form crystals of iPP in the transcrystallized sample (Supporting Information Figure S5). Close examination on the growth front of the TC interphase indicates that the β-form crystals of iPP grow faster than the α-form counterpart (Figure 7a). This observation is consistent with the literature report.[51] When the transcrystallized iPP

DOI: 10.1021/acsami.5b03269
ACS Appl. Mater. Interfaces 2015, 7, 13620−13626

sample was heated up close to 155 °C, the optical birefringence of both α- and β-form crystals increased significantly (Figure 7b). Remarkably, the blue and orange contrast of the mixed birefringence TC interphase changes into the predominant orange contrast of the negative birefringence TC interphase (Figure 7b), indicating a reorientation process of polymer chains at the elevated temperature. As a result, the polymer chains become mainly parallel to the fiber axis, leading to the uniform radial lamellae in the negative birefringence TC interphase.[43] Further increasing the temperature up to 161 °C yielded the melting of the β-form crystals of iPP but no change in the α-form crystals of iPP (Figure 7c,d). This selective melting behavior of the fan-shaped domains further confirmed the β-form crystals of iPP.[50] This observation has not been reported in the single CNT fiber/iPP composites[42,43] or single carbon fiber/iPP composites.[49] It is well-known that the β-form crystals of iPP exhibit the excellent impact strength and toughness that play an important role in fabricating high performance iPP products.[28,52] However, the β-form crystals of iPP are difficult to achieve under the normal processing conditions. Our work indicates the great promise of graphene as an effective reinforcing agent to fabricate strong and tough iPP composites.

To directly visualize microstructures of the TC interphase under SEM, the samples were chemically etched to remove the amorphous regions. Figure 8 displays the typical SEM images of the TC interphase of iPP surrounding the graphene fiber after chemical etching. It is evident that the crystalline lamellae in the TC interphase are oriented perpendicular to the graphene fiber axis while the crystalline lamellae in the bulk spherulite grow radially from the nucleus center (Figure 8a). Close examination of higher magnification images revealed the details of lamellar architectures in both the TC interphase and bulk spherulites (Figure 8b,c). Interestingly, the crystalline lamellae in the TC interphase display interwoven microstructures (Figure 8b), which is termed as a cross-hatched morphology.[42] It is believed that the mother lamellae nucleate on the fiber surface and grow perpendicular to the fiber axis whereas the daughter lamellae (arrows in Figure 8b) epitaxially grow onto the mother lamellae.[42] The epitaxial angle is about 80°. This observation is consistent with those of the single CNT fiber/iPP composites[42] and the single carbon fiber/iPP composites.[49] Figure 8c shows the boundary between the TC interphase and the bulk spherulite, demonstrating the orientation difference of crystalline lamellae between the two.

It should be noted that the graphene fibers are wetted well into the iPP matrix (Figure 8a), implying good interfacial adhesion. However, we did observe some spacing between the TC interphase and the graphene fiber (arrows in Figure 8a). This may be attributed to the mismatch of thermal expansion between the iPP and graphene. During the solidification, the iPP matrix shrinks significantly, producing some spacing between the TC interphase and the graphene fiber. Further investigation is warranted in this context.

CONCLUSIONS

In summary, we have reported polymer transcrystallization of iPP induced by the graphene fibers in the single fiber polymer composites. The graphene fibers are spun from the LC phases of GO sheets followed by chemical reduction. The graphene fibers serve as orientation templates and heterogeneous nucleating agents for promoting the growth of oriented lamellar crystals of iPP perpendicular to the fiber axis. The Lauritzen−Hoffman theory of heterogeneous nucleation is utilized to study the dynamic process of transcrystallization, and the fold surface free energy of transcrystals is calculated to be 5.42×10^{-2} J m^{-2}. The microstructural analysis reveals a cross-hatched morphology of the TC interphase and strong interfacial adhesion. Under the appropriate conditions, the β-form crystals of iPP appear in the predominant α-form transcrystals. Our work addresses an important fundamental issue regarding the interfacial interactions between the polymer and graphene. These results may serve as guidance for the fabrication of effective graphene-enhanced polymer nanocomposites for various emerging applications.

ASSOCIATED CONTENT

Supporting Information

SEM, FTIR, TGA, POM, and XRD. The Supporting Information is available free of charge on the ACS Publications website at DOI: 10.1021/acsami.5b03269.

AUTHOR INFORMATION

Corresponding Author

*Phone: +1 805 756 2591. Fax: +1 805 756 5500. E-mail: szhang05@calpoly.edu.

Notes

The authors declare no competing financial interest.

ACKNOWLEDGMENTS

This work is primarily supported by the Extramural Funding Initiative of Cal Poly. J.P.A. and G.A.B. acknowledge research support from the Bill Moore Research Fellowship of Cal Poly. Y.L., A.R.S., and D.C. acknowledge summer research support from the Frost Research Fellowship of Cal Poly. S.Z. acknowledges financial support from the National Science Foundation (CMMI-1345138) and American Chemical Society-Petroleum Research Fund (53970-UR7).

REFERENCES

(1) Weiss, N. O.; Zhou, H.; Liao, L.; Liu, Y.; Jiang, S.; Huang, Y.; Duan, X. Graphene: An Emerging Electronic Material. *Adv. Mater.* **2012**, *24*, 5782−5825.

(2) Geim, A. K. Graphene: Status and Prospects. *Science* **2009**, *324*, 1530−1534.

(3) Geim, A. K.; Novoselov, K. S. The Rise of Graphene. *Nat. Mater.* **2007**, *6*, 183−191.

(4) Das, T. K.; Prusty, S. Graphene-Based Polymer Composites and Their Applications. *Polym.−Plast. Technol. Eng.* **2013**, *52*, 319−331.

(5) Du, J.; Cheng, H.-M. The Fabrication, Properties, and Uses of Graphene/Polymer Composites. *Macromol. Chem. Phys.* **2012**, *213*, 1060−1077.

(6) Kim, H.; Abdala, A. A.; Macosko, C. W. Graphene/Polymer Nanocomposites. *Macromolecules* **2010**, *43*, 6515−6530.

(7) Potts, J. R.; Dreyer, D. R.; Bielawski, C. W.; Ruoff, R. S. Graphene-Based Polymer Nanocomposites. *Polymer* **2011**, *52*, 5−25.

(8) Sun, X.; Sun, H.; Li, H.; Peng, H. Developing Polymer Composite Materials: Carbon Nanotubes or Graphene? *Adv. Mater.* **2013**, *25*, 5153−5176.

(9) Sun, Y.; Shi, G. Graphene/Polymer Composites for Energy Applications. *J. Polym. Sci., Part B: Polym. Phys.* **2013**, *51*, 231−253.

(10) Xu, J.-Z.; Zhong, G.-J.; Hsiao, B. S.; Fu, Q.; Li, Z.-M. Low-Dimensional Carbonaceous Nanofiller Induced Polymer Crystallization. *Prog. Polym. Sci.* **2014**, *39*, 555−593.

(11) Barber, A. H.; Cohen, S. R.; Wagner, H. D. Measurement of Carbon Nanotube-Polymer Interfacial Strength. *Appl. Phys. Lett.* **2003**, *82*, 4140−4142.

DOI: 10.1021/acsami.5b03269
ACS Appl. Mater. Interfaces 2015, 7, 13620−13626

(12) Liu, Y.; Kumar, S. Polymer/Carbon Nanotube Nano Composite Fibers-a Review. *ACS Appl. Mater. Interfaces* **2014**, *6*, 6069−6087.
(13) Chen, X.; Zheng, M.; Park, C.; Ke, C. Direct Measurements of the Mechanical Strength of Carbon Nanotube-Poly(Methyl Methacrylate) Interfaces. *Small* **2013**, *9*, 3345−3351.
(14) Zhang, S.; Lin, W.; Wong, C.-P.; Bucknall, D. G.; Kumar, S. Nanocomposites of Carbon Nanotube Fibers Prepared by Polymer Crystallization. *ACS Appl. Mater. Interfaces* **2010**, *2*, 1642−1647.
(15) Zhang, S.; Zhu, L.; Wong, C.-P.; Kumar, S. Polymer-Infiltrated Aligned Carbon Nanotube Fibers by in Situ Polymerization. *Macromol. Rapid Commun.* **2009**, *30*, 1936−1939.
(16) Zhang, S.; Lin, W.; Yu, X.; Wong, C.-P.; Cheng, S. Z. D.; Bucknall, D. G. Surface-Induced Polymer Crystallization in High Volume Fraction Aligned Carbon Nanotube-Polymer Composites. *Macromol. Chem. Phys.* **2010**, *211*, 1003−1011.
(17) Li, L.; Li, B.; Hood, M. A.; Li, C. Y. Carbon Nanotube Induced Polymer Crystallization: The Formation of Nanohybrid Shish-Kebabs. *Polymer* **2009**, *50*, 953−965.
(18) Ma, J.; Meng, Q.; Michelmore, A.; Kawashima, N.; Izzuddin, Z.; Bengtsson, C.; Kuan, H.-C. Covalently Bonded Interfaces for Polymer/Graphene Composites. *J. Mater. Chem. A* **2013**, *1*, 4255−4264.
(19) Zhang, Y.; Wang, Y.; Yu, J.; Chen, L.; Zhu, J.; Hu, Z. Tuning the Interface of Graphene Platelets/Epoxy Composites by the Covalent Grafting of Polybenzimidazole. *Polymer* **2014**, *55*, 4990−5000.
(20) Vasileiou, A. A.; Kontopoulou, M.; Docoslis, A. A Noncovalent Compatibilization Approach to Improve the Filler Dispersion and Properties of Polyethylene/Graphene Composites. *ACS Appl. Mater. Interfaces* **2014**, *6*, 1916−1925.
(21) Sun, Y.; He, C. Synthesis and Stereocomplex Crystallization of Poly(Lactide)-Graphene Oxide Nanocomposites. *ACS Macro Lett.* **2012**, *1*, 709−713.
(22) Cheng, S.; Chen, X.; Hsuan, Y. G.; Li, C. Y. Reduced Graphene Oxide-Induced Polyethylene Crystallization in Solution and Nanocomposites. *Macromolecules* **2012**, *45*, 993−1000.
(23) Xu, J.-Z.; Liang, Y.-Y.; Zhong, G.-J.; Li, H.-L.; Chen, C.; Li, L.-B.; Li, Z.-M. Graphene Oxide Nanosheet Induced Intrachain Conformational Ordering in a Semicrystalline Polymer. *J. Phys. Chem. Lett.* **2012**, *3*, 530−535.
(24) Xu, J.-Z.; Chen, C.; Wang, Y.; Tang, H.; Li, Z.-M.; Hsiao, B. S. Graphene Nanosheets and Shear Flow Induced Crystallization in Isotactic Polyproylene Nanocomposites. *Macromolecules* **2011**, *44*, 2808−2818.
(25) Xu, P.; Loomis, J.; Bradshaw, R. D.; Panchapakesan, B. Load Transfer and Mechanical Properties of Chemically Reduced Graphene Reinforcements in Polymer Composites. *Nanotechnology* **2012**, *23*, 505713.
(26) Jang, H.-K.; Kim, H.-I.; Dodge, T.; Sun, P.; Zhu, H.; Nam, J.-D.; Suhr, J. Interfacial Shear Strength of Reduced Graphene Oxide Polymer Composites. *Carbon* **2014**, *77*, 390−397.
(27) Rafiee, M. A.; Rafiee, J.; Wang, Z.; Song, H.; Yu, Z.-Z.; Koratkar, N. Enhanced Mechanical Properties of Nanocomposites at Low Graphene Content. *ACS Nano* **2009**, *3*, 3884−3890.
(28) Quan, H.; Li, Z. M.; Yang, M. B.; Huang, R. On Transcrystallinity in Semi-Crystalline Polymer Composites. *Compos. Sci. Technol.* **2005**, *65*, 999−1021.
(29) Xu, H.; Xie, L.; Jiang, X.; Li, X.-J.; Li, Y.; Zhang, Z.-J.; Zhong, G.-J.; Li, Z.-M. Toward Stronger Transcrystalline Layers in Poly(L-Lactic Acid)/Natural Fiber Biocomposites with the Aid of an Accelerator of Chain Mobility. *J. Phys. Chem. B* **2014**, *118*, 812−823.
(30) Zhou, M.; Xu, S.; Li, Y.; He, C.; Jin, T.; Wang, K.; Deng, H.; Zhang, Q.; Chen, F.; Fu, Q. Transcrystalline Formation and Properties of Polypropylene on the Surface of Ramie Fiber as Induced by Shear or Dopamine Modification. *Polymer* **2014**, *55*, 3045−3053.
(31) Wen, T.; Zhang, X.; Xiong, Z.; de Vos, S.; Wang, R.; Wang, F.; Wang, D. Study on Fracture Behavior of Plla Transcrystallization: Effect of Crystalline Morphology. *J. Appl. Polym. Sci.* **2015**, *132*.
(32) Li, H.; Yan, S. Surface-Induced Polymer Crystallization and the Resultant Structures and Morphologies. *Macromolecules* **2011**, *44*, 417−428.
(33) Li, H. H.; Jiang, S. D.; Wang, J. J.; Wang, D. J.; Yan, S. K. Optical Microscopic Study on the Morphologies of Isotactic Polypropylene Induced by Its Homogeneity Fibers. *Macromolecules* **2003**, *36*, 2802−2807.
(34) Xu, Z.; Gao, C. Graphene in Macroscopic Order: Liquid Crystals and Wet-Spun Fibers. *Acc. Chem. Res.* **2014**, *47*, 1267−1276.
(35) Xiang, C.; Young, C. C.; Wang, X.; Yan, Z.; Hwang, C.-C.; Cerioti, G.; Lin, J.; Kono, J.; Pasquali, M.; Tour, J. M. Large Flake Graphene Oxide Fibers with Unconventional 100% Knot Efficiency and Highly Aligned Small Flake Graphene Oxide Fibers. *Adv. Mater.* **2013**, *25*, 4592−4597.
(36) Jalili, R.; Aboutalebi, S. H.; Esrafilzadeh, D.; Shepherd, R. L.; Chen, J.; Aminorroaya-Yamini, S.; Konstantinov, K.; Minett, A. I.; Razal, J. M.; Wallace, G. G. Scalable One-Step Wet-Spinning of Graphene Fibers and Yarns from Liquid Crystalline Dispersions of Graphene Oxide: Towards Multifunctional Textiles. *Adv. Funct. Mater.* **2013**, *23*, 5345−5354.
(37) Luo, Y.; Braggin, G. A.; Olson, G. T.; Stevenson, A. R.; Ruan, W. L.; Zhang, S. Nematic Order Drives Macroscopic Patterns of Graphene Oxide in Drying Drops. *Langmuir* **2014**, *30*, 14631−14637.
(38) Hummers, W. S.; Offeman, R. E. Preparation of Graphitic Oxide. *J. Am. Chem. Soc.* **1958**, *80*, 1339−1339.
(39) Zhang, S.; Majewski, P. W.; Keskar, G.; Pfefferle, L. D.; Osuji, C. O. Lyotropic Self-Assembly of High-Aspect-Ratio Semiconductor Nanowires of Single-Crystal Zno. *Langmuir* **2011**, *27*, 11616−11621.
(40) Kim, J. E.; Han, T. H.; Lee, S. H.; Kim, J. Y.; Ahn, C. W.; Yun, J. M.; Kim, S. O. Graphene Oxide Liquid Crystals. *Angew. Chem., Int. Ed.* **2011**, *50*, 3043−3047.
(41) Xu, Z.; Gao, C. Aqueous Liquid Crystals of Graphene Oxide. *ACS Nano* **2011**, *5*, 2908−2915.
(42) Zhang, S.; Minus, M. L.; Zhu, L.; Wong, C.-P.; Kumar, S. Polymer Transcrystallinity Induced by Carbon Nanotubes. *Polymer* **2008**, *49*, 1356−1364.
(43) Gao, Y.; Xie, M.; Liu, L.; Li, J.; Kuang, J.; Ma, W.; Zhou, W.; Xie, S.; Zhang, Z. Effect of Supra-Molecular Microstructures on the Adhesion of Swcnt Fiber/Ipp Interface. *Polymer* **2013**, *54*, 456−463.
(44) Wang, S.; Zhang, Y.; Abidi, N.; Cabrales, L. Wettability and Surface Free Energy of Granene Films. *Langmuir* **2009**, *25*, 11078−111081.
(45) Cho, K.; Kim, D.; Yoon, S. Effect of Substrate Surface Energy on Transcrystalline Growth and Its Effect on Interfacial Adhesion of Semicrystalline Polymers. *Macromolecules* **2003**, *36*, 7652−7660.
(46) Luo, Y.; Santos, F. A.; Wagner, T. W.; Tsoi, E.; Zhang, S. Dynamic Interactions between Poly(3-Hexaylthiophene) and Single-Walled Carbon Nanotubes in Marginal Solvent. *J. Phys. Chem. B* **2014**, *118*, 6038−6046.
(47) Hoffman, J. D.; Miller, R. L. Kinetics of Crystallization from the Melt and Chain Folding in Polyethylene Fractions Revisited: Theory and Experiment. *Polymer* **1997**, *38*, 3151−3212.
(48) Clark, E. J.; Hoffman, J. D. Regime-III Crystallization in Polypropylene. *Macromolecules* **1984**, *17*, 878−885.
(49) Assouline, E.; Pohl, S.; Fulchiron, R.; Gerard, J. F.; Lustiger, A.; Wagner, H. D.; Marom, G. The Kinetics of Alpha and Beta Transcrystallization in Fibre-Reinforced Polypropylene. *Polymer* **2000**, *41*, 7843−7854.
(50) Sun, X.; Li, H.; Wang, J.; Yan, S. Shear-Induced Interfacial Structurs of Isotactic Polypropylene (Ipp) in Ipp/Fiber Composites. *Macromolecules* **2006**, *39*, 8720−8726.
(51) Sun, X.; Li, H.; Zhang, X.; Wang, D.; Schultz, J. M.; Yan, S. Effect of Matrix Molecular Mass on the Crystallization of Beta Form Isotactic Polypropylene around an Oriented Polypropylene Fiber. *Macromolecules* **2010**, *43*, 561−564.
(52) Bai, H.; Wang, Y.; Zhang, Z.; Han, L.; Li, Y.; Liu, L.; Zhou, Z.; Men, Y. Influence of Annealing on Microstructure and Mechanical Properties of Isotactic Polypropylene with Beta-Phase Nucleating Agen. *Macromolecules* **2009**, *42*, 6647−6655.

DOI: 10.1021/acsami.5b03269
ACS Appl. Mater. Interfaces 2015, 7, 13620−13626